SCIENTIFIC REPORTS

OPEN

SUBJECT AREAS:
METALS AND ALLOYS
IMAGING TECHNIQUES
STRUCTURE OF SOLIDS AND LIQUIDS
PHASE TRANSITIONS AND CRITICAL PHENOMENA

Received
29 January 2013

Accepted
29 May 2013

Published
19 June 2013

Correspondence and requests for materials should be addressed to A.C. (aclarke@lanl.gov)

Proton Radiography Peers into Metal Solidification

Amy Clarke[1], Seth Imhoff[1], Paul Gibbs[1], Jason Cooley[1], Christopher Morris[1], Frank Merrill[1], Brian Hollander[1], Fesseha Mariam[1], Thomas Ott[1], Martha Barker[1], Tim Tucker[1], Wah-Keat Lee[2], Kamel Fezzaa[3], Alex Deriy[3], Brian Patterson[1], Kester Clarke[1], Joel Montalvo[1], Robert Field[1], Dan Thoma[1], James Smith[1] & David Teter[1]

[1]Los Alamos National Laboratory, P.O. Box 1663, Los Alamos, NM 87545, [2]Brookhaven National Laboratory, P.O. Box 5000, Upton, NY 11973, [3]Argonne National Laboratory, 9700 South Cass Avenue, Argonne, IL 60439.

Historically, metals are cut up and polished to see the structure and to infer how processing influences the evolution. We can now peer into a metal during processing without destroying it using proton radiography. Understanding the link between processing and structure is important because structure profoundly affects the properties of engineering materials. Synchrotron x-ray radiography has enabled real-time glimpses into metal solidification. However, x-ray energies favor the examination of small volumes and low density metals. Here we use high energy proton radiography for the first time to image a large metal volume (>10,000 mm³) during melting and solidification. We also show complementary x-ray results from a small volume (<1 mm³), bridging four orders of magnitude. Real-time imaging will enable efficient process development and the control of structure evolution to make materials with intended properties; it will also permit the development of experimentally informed, predictive structure and process models.

Imaging of natural phenomena often reveals unknown truths and transforms our scientific perspectives. Prompted by a bet in the late 1800s, Eadweard James Muybridge sought to capture the running of horses on film to see if all four hooves left the ground simultaneously[1]. His image sequences confirmed this occurrence for the first time, which ultimately resulted in his career studying the motion of animals[1–3]. Similarly, in a career spanning over four decades, Wilson A. Bentley imaged over 5,000 different crystalline snowflakes, revealing astonishing variations in snowflake structure[4–8]. In November 1895, Wilhelm Conrad Röntgen discovered x-rays, which immediately revolutionized physics and medicine, as the penetration of x-rays allows for x-ray (or radiographic) static imaging to nondestructively interrogate the inside of the human body or materials[9–12]. Today, real-time imaging of small volumes and low density metals during solidification is possible using brilliant synchrotron x-ray sources available at user facilities around the world[13–33]. We show that proton radiography has the potential to revolutionize solidification science in similar ways.

Pure metals solidify at a single temperature, whereas metallic alloys solidify over a range of temperatures and compositions. For a hypothetical dilute binary alloy, the equilibrium concentrations of solute in the liquid and solid phases are defined for a given temperature. However, since the reaction takes place over a range of temperatures, the equilibrium conditions change continuously during solidification, so that only local interfacial equilibrium is maintained and the solute environment close to the interface is determined by the relative rates of mass transport in the solid and liquid phases. In many systems there is only one liquid solution and the transport in the liquid phase is fast with respect to diffusion in the solid phase. Solubility of the solute in the solid phase usually increases with decreasing temperature, but solid-state diffusion is too slow to equilibrate the solid, so the liquid becomes enriched in solute. The temperature gradient, concentration gradient, and the growth velocity determine the interfacial morphology and can result in pattern formation, such as branched dendritic structures like the arms of a snowflake (i.e. dendrites). In systems where multiple immiscible liquid phases exist, such as in the aluminum-indium (Al-In) alloy system, similar solute pile-up can occur, but the interfacial stability conditions of the growing solid phase are altered.

Manipulation of solidification parameters is crucial for growing single crystals or controlling structure evolution and micro-segregation in a casting, setting the stage for what properties are possible after any downstream processing. Large scale parameters are controlled by casting design, which can include highly engineered melt flow patterns, heat transfer during mold filling, and progression of the solidification reaction. Ultimately, this early processing path determines the overall quality of a casting by influencing the presence of defects (e.g.

dimensional tolerance, composition segregation, or void formation) and the microscopic phase arrangement – characteristics that persist even after subsequent thermal-mechanical processing (e.g. heat-treatment and forging). Current methods to design castings incorporate experimental trials with destructive characterization techniques and empirical modeling. Post-mortem structure evaluations are typically used to infer what occurred at elevated temperatures, but direct observations of metallic alloy solidification have been limited. More importantly, commercially available tools to simulate fluid flow and solidification sequence are generally finite-element based and rely largely on post-processing and empirical relationships to simulate structural outcomes. However, real-time monitoring of metallic alloys during processing will now permit direct interrogation of responses to parameter changes needed to develop predictive structure evolution models to couple with finite elements and bridge the micro- and macro-scale regimes. It will also enable directed synthesis and processing to control structure evolution and the creation of optimal properties during process development.

Results

The Los Alamos Neutron Science Center (LANSCE) at Los Alamos National Laboratory (LANL) is home to a powerful 800 mega-electron-volt (MeV) proton linear accelerator (LINAC). Modern proton radiography was invented at LANL to use 800 MeV protons for multi-frame flash radiography for dynamic (explosively driven) materials studies[34–36]. Proton radiography (pRad) is similar to x-ray radiography in that it produces a projected image; however, pRad uses protons rather than x-rays to directly probe and image dynamic behavior. A collimator is placed at the Fourier plane of the proton imaging system to generate contrast in the proton radiograph by removing protons scattered into a specified angular range. The collimation can be adjusted to optimize image contrast for a wide range of object thicknesses, corresponding to sample densities from 200 mg/cm^2 to 50 g/cm^2. This technique has been optimized over the years and achieves ~1% density resolution with typical exposure times of 100 ns during dynamic experiments[37]. At 800 MeV, proton image resolution is limited by chromatic aberrations of the protons, focused by the magnetic imaging lens, and the resolution of the detector system. To overcome these effects, magnifying imaging lenses have been designed to reduce chromatic aberrations and increase magnification that are placed between the object and the detection system[38]. This improves the resolution of the system by both reducing chromatic aberrations and scaling the field of view to the experimental region of interest. These improvements have been demonstrated through performance measurements using an X3 magnifier system, with a nominal spatial resolution of 65 μm[39]. Exposure times of seconds are reasonable for imaging bulk solidification and are easily achieved at pRad. We have used pRad for the first time to directly image bulk metallic alloy melting and solidification in thick (2–6 mm) sections and a substantial field of view (~44 × 44 mm) using the X3 magnifier over times ranging from minutes to hours. LANSCE is uniquely suited for our bulk material studies.

Here we present the results of melting and solidification experiments in the Al-In alloy system. An ambient pressure, equilibrium phase diagram[40] is provided in Figure 1. At the alloy composition Al-4.7 at.% In, the monotectic reaction $L \rightarrow Al_S + L_2$ occurs at 636.5 °C. For hypermonotectic alloy compositions (above 4.7 at.% In), a range of compositions and temperatures exist where two immiscible liquids, $L_1 + L_2$, co-exist. This region of the phase diagram is known as a miscibility gap. We selected a hypermonotectic Al-10 at.% In alloy composition for our in-situ characterization of metallic alloy melting and solidification, with the intent of creating a fraction of indium-rich (In-rich) L_2 liquid droplets distinguishable from the majority aluminum-rich (Al-rich) L_1 liquid phase at elevated temperatures. Given the density difference between these two immiscible liquid phases[41], sufficient contrast is available for the study of L_1/L_2 fluid flow using radiography. Monitoring of the solid-liquid interface is also possible.

pRad affords investigations of thick samples (and large volumes), which is an advantage for studying inherently three-dimensional problems like casting or fluid flow. It also affords investigations of high density metallic alloys during processing that may not be possible with x-rays, given energy and sample geometry restrictions. Given our interest in connecting bulk to microscopic solidification behavior, we chose to examine a thick section. A select series of images from the first ever pRad video sequence (see Supplementary Information Video S1) of Al-10 at.% In during melting and solidification is shown in Figure 2 for a 6 mm thick section. This

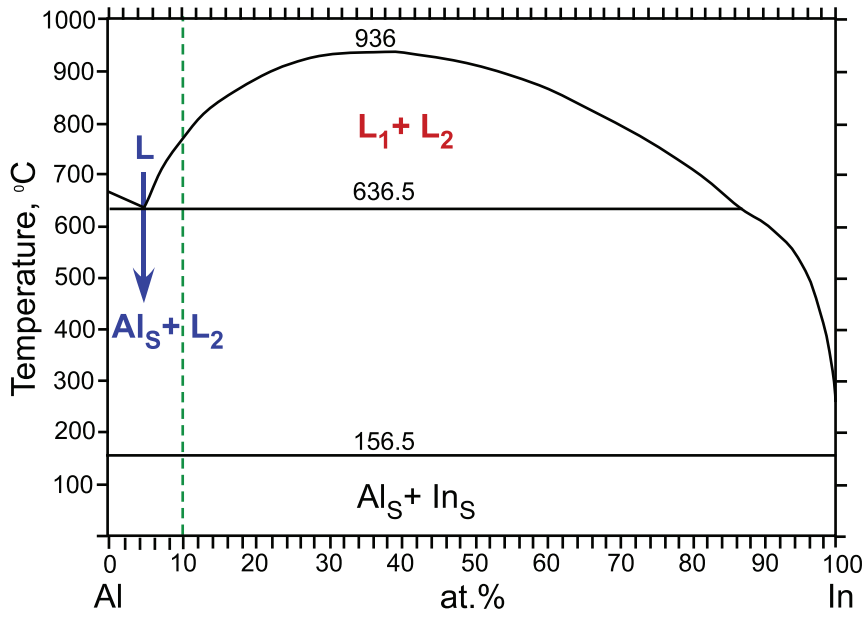

Figure 1 | Equilibrium phase diagram for the Al-In alloy system[40] that undergoes the monotectic reaction $L \rightarrow Al_S + L_2$ (denoted in blue) at the temperature 636.5 °C. Two immiscible liquids, $L_1 + L_2$ (denoted in red), co-exist over a range of temperatures and compositions. The nominal alloy composition, Al-10 at.% In, studied here is highlighted by the green dashed line.

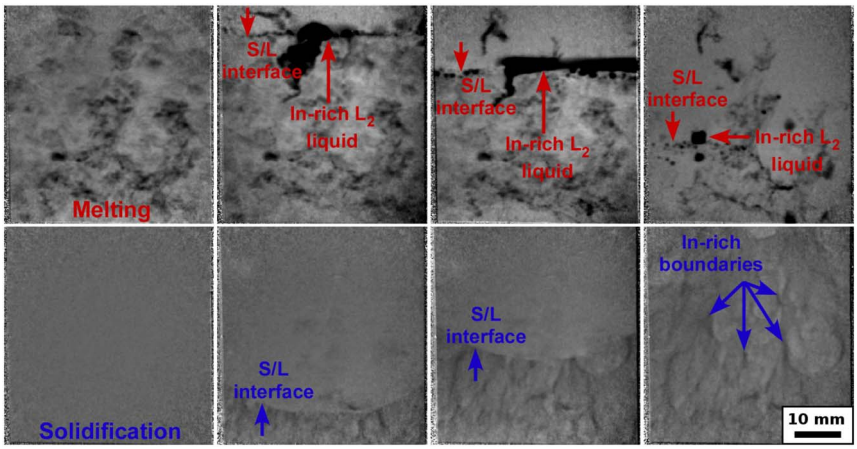

Figure 2 | Selected images from the first ever proton radiography sequence of melting (upper images) and solidification (lower images) in a 6 mm thick Al-10 at.% In section. The In-rich L_2 liquid phase appears dark. The monotectic reaction is observed during solidification because macro-scale sedimentation of the denser In-rich L_2 liquid phase occurs during melting. The corresponding video (Supplementary Information Video S1) shows the melting and solidification progression.

large section size permits bulk analysis, allowing for interrogation of the meso- and macro- length scales relevant in casting. Melting progresses from the top downward, and larger In-rich regions are released during liquification of the surrounding solid aluminum. Large volumes of the denser In-rich L_2 liquid phase (dark contrast in the images) tend to remain close to the solid-liquid interface during melting due to gravity. Coalescence of In-rich regions is also observed. Fine droplets of the In-rich liquid remain in suspension and flow within the majority L_1 liquid phase, eventually dissolving at elevated temperatures. However, the average composition of the alloy in the field of view becomes lean relative to the nominal Al-10 at.% In composition after melting because of In-rich L_2 liquid phase sedimentation, shifting it closer to the monotectic composition (4.7 at.% In). Essentially, macro-segregation in the form of an In-rich sediment layer exists at the bottom of the crucible. This phenomenon makes casting hypermonotectic alloys challenging[21,22].

Advancement of the solid-liquid interface is shown in the representative solidification sequence images. The solid-liquid interface advances at an average growth velocity of approximately 200 μm/s in the vertical direction (antiparallel to the global heat flow direction). The growth velocity actually varies somewhat from the edge to the center of the field of view due to heat extraction from the edges of the crucible, which is reflected in the interface shape. These images also highlight the monotectic reaction during solidification and reveal the spatial distribution of meso-scale monotectic colonies. The darker streaks observed in the pRad images (Figure 2) correspond to a projection through colony boundaries that contain a higher volume fraction of indium. Although we selected a 6 mm thick section for our pRad study, pRad also affords the flexibility to examine thinner, constrained sections. This might reduce potential projection issues associated with thicker sections, but if three-dimensional information is required for a particular study, proton tomography[42] (like x-ray tomography[23,29,30,32,33]) is possible. If only some three-dimensional information is desired, additional radiographs taken at select rotations would afford construction of a stereo image. Microstructural features observed during microscopic examination of ex-situ serial sections from our pRad field of view are consistent with those we observe in pRad images, suggesting that through-thickness projection is not a major concern in our study aimed at monitoring macro- and mesoscale fluid flow. An area containing representative In-rich boundaries in a pRad image is highlighted in Figure 3(a); a higher magnification post-mortem scanning electron microscopy image of that region is shown in Figure 3(b), along with an even higher magnification image in Figure 3(c). Here, the In-rich boundaries and regions within the colonies appear bright and exist in two size classes – either as high aspect ratio fibers or as low aspect ratio droplets. These regions contain a fine-scale Al-rich phase, presumably associated with solute separation as aluminum solubility in L_2 decreases during cooling from the monotectic reaction (the invariant reaction at 636.5°C). The images in Figure 3 reflect the coupled complexities of structure evolution that transpired at a variety of length scales in this alloy system.

Macroscopic fluid currents exist in the alloy melt, as evidenced by sedimentation during melting in Figure 2, in concert with meso- and micro-scale flows that are influenced by external fields (i.e. gravity, thermo-capillarity, or Stokes drag forces acting on second phase

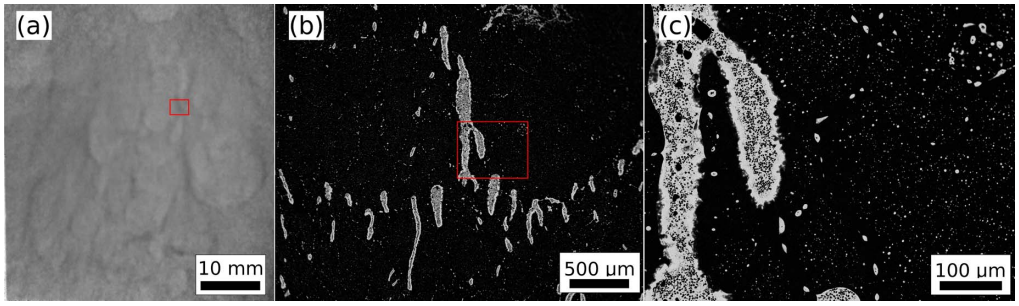

Figure 3 | (a) A proton radiography image (Figure 2) of the solidification structure and (b,c) corresponding post-mortem scanning electron microscopy of the indicated regions that highlight the In-rich boundaries and regions that exist within the colonies of the solidified structure. In (a), the higher density In-rich boundaries appear dark, whereas the In-rich boundaries and regions appear bright in (b,c). The In-rich boundaries and regions in (b) and (c) contain a fine-scale Al-rich (dark) phase.

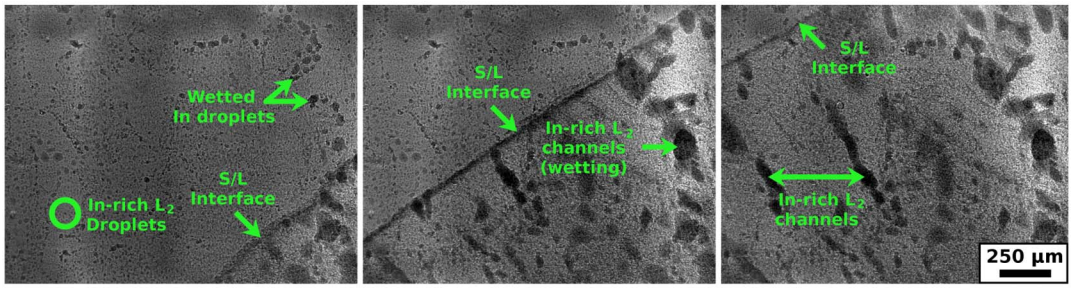

Figure 4 | Selected images from a synchrotron x-ray radiography sequence of solidification in a 0.2 mm thick Al-10 at.% In section, highlighting In-rich L_2 liquid phase (dark) along the solid-liquid interface and In-rich L_2 channel development. In addition to the solidification progression, the corresponding video (Supplementary Information Video S2) reveals In-rich droplet motion and coarsening within the majority L_1 liquid phase.

droplets[21,22]). These flows affect morphological evolution during solidification. To reveal dynamic processes occurring in Al-10 at.% In during melting and solidification at smaller length scales, we performed complementary synchrotron x-ray radiography, imaging approximately a 1.4 × 1.74 mm field of view in a 0.2 mm thick section, at the Sector 32-Insertion Device beamline at Argonne National Laboratory's Advanced Photon Source. It is important to reiterate that the sample volume interrogated using x-rays is over four orders of magnitude smaller than that probed using protons at pRad. A series of images from an x-ray solidification sequence is shown in Figure 4. An accompanying video (see Supplementary Information Video S2) highlights L_1/L_2 fluid flow, including the formation, coarsening (ripening and coalescence), and complex collective motion of In-rich L_2 droplets within the majority L_1 liquid phase at elevated temperatures. In a constant but small thermal gradient, the droplet motion is highly irregular, with larger scale convective currents sweeping in and out of the field of view. Once the monotectic front approaches the field of view, more organized motion begins to dominate. During solidification, L_2 droplets are on a trajectory toward the advancing solid-liquid interface (see Figure 4 and the accompanying Supplementary Information Video S2). These L_2 droplets accumulate at the solid-liquid interface and are either pushed along that interface, or are engulfed in the solidifying Al matrix, creating In-rich channels (Figure 4). The same physics observed by Schaffer *et al.*[21] in an x-ray study of the Al-Bi system apply to droplet motion in our study; however, more chaotic convection currents appear to exist in our samples during cooling. The solid-liquid interface advances at a growth velocity of approximately 145 µm/s. The x-ray images also suggest that indium wets the crucible walls in some instances, which promotes the formation of In-rich channels at these locations. Hydrodynamic effects of the L_2 liquid phase exist at the micro-, meso-, and macro- length scales in this hypermonotectic alloy and substantially influence the resulting solidification structure. Improved understanding of micro- and meso-scale L_2 droplet motion may provide a methodology to advantageously control alloy melt flows in these alloys to offset macro-scale sedimentation and improve casting quality[21,22].

Discussion

We have demonstrated that the ability to interrogate large volumes (pRad) in metallic alloys during solidification and complement these results with local, higher resolution (x-ray) observations allows for unprecedented understanding of fluid flow and structure development. Experiments such as these will revolutionize our knowledge of metal casting and completely transform our ability to model these phenomena accurately. Furthermore, interest exists among the physics and materials communities to move toward higher energy proton radiography, which will provide improved spatial resolution and make protons an ideal probe for two- and three-dimensional simultaneous macro- and micro- length scale solidification studies in low or high density metallic alloys. Process parameters such as thermal gradient and solid-liquid interface velocity affect the solid-liquid interface stability in metallic alloys during solidification, which can result in pattern-forming instabilities that dictate the morphological and structure evolution. Real-time feedback from in-situ characterization will permit in-process parameter changes to control structure and defect evolution to achieve desired properties and the development of experimentally informed, predictive multi-scale models for solidification and structure evolution. In-situ characterization, in particular proton radiography, will also enable process-aware manufacturing studies of materials, reducing the time for process development and the time from discovery to deployment through the elimination of trial and error, which are critical for advanced manufacturing initiatives[43–45].

Proton microscopy fills a critical gap in the evolving capabilities of dynamic imaging techniques. Specifically, it allows for direct observations of structural outcomes as a function of processing in large volumes of materials; it also affords studies of three-dimensional processes, such as fluid flow encountered during solidification for which thick sections, rather than thin (constrained) sections, ultimately better represent processes that occur in actual castings. Performance measurements at pRad have successfully demonstrated an X7 microscope configuration with nominal spatial resolution of ~17 µm for a ~17 × 17 mm field of view[46,47]; we are currently pursuing improved spatial resolution for our studies, beyond the low magnification results shown here that were acquired using the X3 magnifier. We have also successfully demonstrated that we can acquire tomographic reconstructions of morphological evolution in metallic alloys during solidification using x-rays[33], which is also possible at pRad. Proton radiography is a unique, in-situ characterization tool with significant potential that finally connects the macro-scale to the micro-scale, which will permit the exploration of efficient processing to produce materials with intended structures and properties[44,45].

Methods

Sample preparation. Charges of aluminum and indium were loaded into small graphite crucibles encapsulated in quartz and backfilled with argon and melted in a furnace. These samples were cold-rolled to ~2 or ~0.2 mm in thickness. A stack of 2 mm thick sheets was re-heated in a large graphite crucible in a vacuum furnace at 670 °C for 3 hr to create a single 6 mm thick sample with a coarse starting structure for proton radiography. The 0.2 mm thick foil was used for x-ray radiography.

800 MeV proton radiography at Los Alamos National Laboratory's Los Alamos Neutron Science Center. The 6 mm thick sample, nominally 112 mm in width by 108 mm in height, was heated in a large graphite crucible embedded with thermocouples at 1.5 °C/min with a 2 °C/cm applied gradient. A centered window (~50 × 50 mm) with reduced thickness was machined into the front and back of the crucible. A 305 × 305 mm aluminum box with machined windows contained the crucible. The crucible was resistively heated by adjacent graphite blocks situated next to water-cooled copper blocks. The entire system was under vacuum. Images were obtained from the windowed region during heating and cooling in video mode.

Synchrotron x-ray radiography at the Sector 32-Insertion Device beamline at Argonne National Laboratory's Advanced Photon Source. A 5 mm diameter disk

of 0.2 mm thick foil was sprayed with boron-nitride. The disk was inserted into a quartz frame sandwiched between two ~25 × 12.5 × 0.25 mm quartz slides. The edges were sealed, and this configuration was inserted into a slotted 12.7 mm diameter graphite rod with a through hole embedded with thermocouples. Induction coils above and below the sample were used for heating. The x-ray energy was 18 keV. Real-time images were acquired with exposure times of 0.04 s and a frame rate of ~4.5 s^{-1}.

1. Miller, A. (October 2000), revised by Hemsath, D. (October 2004). Penn University Archives & Records Center, Archival Collections, Eadweard Muybridge, 1830–1904, Collection, 1870–1981.Retrieved November 20, 2012, from http://www.archives.upenn.edu/faids/upt/upt50/muybridgee.html.
2. Munn, O. D. & Beach, A. E. A horse's motion scientifically determined. *Scientific American* **39**(16), 241 (1878).
3. Muybridge, E. *Descriptive Zoopraxography or the Science of Animal Locomotion,* The Lakeside Press, R. R. Donneley & Sons Co., Chicago, IL, 1893.
4. Art Institute Chicago, Wilson A. Bentley, Snowflake, 1885/1931. Retrieved December 5, 2012, from http://www.artic.edu/aic/collections/artwork/203080?search_no=1&index=0.
5. Bentley, W. A. Twenty years study of snow crystals. *Monthly Weather Review* **29**(5), 212–214 (1901).
6. Willey, D. A. Snow crystals. *Scientific American* **92**(2), 21–22 (1905).
7. Bentley, W. A. Forty years study of snow crystals. *Monthly Weather Review* **52**(11), 530–532 (1924).
8. Bentley, W. A. Some recent treasures of the snow. *Monthly Weather Review* **55**(8), 358–359 (1927).
9. Röntgen, W. C. Translated by Arthur Stanton from the Sitzungsberichte der Würzburger Physik-medic. Gesellschaft, 1895. On a new kind of rays. *Nature* **53**(1369), 274–276 (1896).
10. Kaye, G. W. C. Wilhelm Conrad Röntgen: and the early history of the Roentgen rays. *Nature* **133**(3362), 511–513 (1934).
11. Farmelo, G. The discovery of x-rays. *Scientific American* **273**(5), 86–91 (1995).
12. Seliger, H. H. Wilhelm Conrad Röntgen and the glimmer of light. *Physics Today* **48**(11), 25–31 (1995).
13. Mathiesen, R. H. *et al.* Time-resolved x-ray imaging of aluminum alloy solidification processes. *Metallurgical and Materials Transactions B* **33B**, 613–623 (2002).
14. Mathiesen, R. H. & Arnberg, L. Stray crystal formation in Al-20 wt.% Cu studied by synchrotron x-ray video microscopy. *Materials Science and Engineering A* **413–414**, 283–287 (2005).
15. Mathiesen, R. H. & Arnberg, L. X-ray radiography observations of columnar dendritic growth and constitutional undercooling in an Al-30wt.%Cu alloy. *Acta Materialia* **53**, 947–956 (2005).
16. Mathiesen, R. H., Arnberg, L., Bleuet, P. & Somogyi, A. Crystal fragmentation and columnar-to-equiaxed transitions in Al-Cu studied by synchrotron x-ray video microscopy. *Metallurgical and Materials Transactions A* **37A**, 2515–2524 (2006).
17. Arnberg, L. & Mathiesen, R. H. The real-time, high-resolution x-ray video microscopy of solidification in aluminum alloys. *JOM* **59**(8), 20–26 (2007).
18. Ruvalcaba, D., Mathiesen, R. H., Eskin, D. G., Arnberg, L. & Katgerman, L. In situ observations of dendritic fragmentation due to local solute-enrichment during directional solidification of an aluminum alloy. *Acta Materialia* **55**, 4287–4292 (2007).
19. Nguyen-Thi, H. *et al.* In-situ and real-time investigation of columnar-to-equiaxed transition in metallic alloy. *Metallurgical and Materials Transactions A* **38A**, 1458–1464 (2007).
20. Reinhart, G. *et al.* In-situ and real-time analysis of the formation of strains and microstructure defects during solidification of Al-3.5 wt. pct Ni alloys. *Metallurgical and Materials Transactions A* **39A**, 865–874 (2008).
21. Schaffer, P. L., Mathiesen, R. H., Arnberg, L., Di Sabatino, M. & Snigirev, A. In situ investigation of spinodal decomposition in hypermonotectic Al-Bi and Al-Bi-Zn alloys. *New Journal of Physics* **10**(053001), 1–16 (2008).
22. Schaffer, P. L., Mathiesen, R. H. & Arnberg, L. L_2 droplet interaction with α-Al during solidification of hypermonotectic Al-8wt.%Bi alloys. *Acta Materialia* **57**, 2887–2895 (2009).
23. Limodin, N. *et al.* In-situ and real-time 3-D microtomography investigation of dendritic solidification in an Al-10wt.%Cu alloy. *Acta Materalia* **57**, 2300–2310 (2009).
24. Bogno, A. *et al.* Analysis by synchrotron x-ray radiography of convection effects on the dynamic evolution of the solid-liquid interface and on solute distribution during the initial transient of solidification. *Acta Materialia* **59**, 4356–4365 (2011).
25. Bogno, A. *et al.* In situ analysis of the influence of convection during the initial transient of planar solidification. *Journal of Crystal Growth* **318**, 1134–1138 (2011).
26. Chen, Y. *et al.* Quantitatively comparing phase-field modeling with direct real-time observation by synchrotron x-ray radiography of the initial transient during directional solidification of an Al-Cu alloy. *Acta Materialia* **60**, 199–207 (2012).
27. Phillion, A. B. In-situ observation of solidification phenomena. *JOM* **64**(1), 66–67 (2012).
28. Mathiesen, R. H., Arnberg, L., Nguyen-Thi, H. & Billia, B. In-situ x-ray video microscopy as a tool in solidification science. *JOM* **64**(1), 76–82 (2012).
29. Suery, M. *et al.* Fast in-situ x-ray microtomography observations of solidification and semisolid deformation of Al-Cu alloys. *JOM* **64**(1), 83–88 (2012).
30. Puncreobutr, C., Lee, P. D., Hamilton, R. W. & Phillion, A. B. Quantitative 3D characterization of solidification structure and defect evolution in Al alloys. *JOM* **64**(1), 89–95 (2012).
31. Grujic, K., Hegna, T. & Laundal, K. N. In-situ monitoring of growth interfaces: a review of noninvasive methods. *JOM* **64**(1), 96–101 (2012).
32. Rowenhorst, D. J. & Voorhees, P. W. Measurement of interfacial evolution in three dimensions. *Annual Review of Materials Research* **42**, 105–124 (2012).
33. Clarke, A. J. *et al.* X-ray imaging of Al-7at.%Cu during melting and solidification. *Emerging Materials Research* **2**(EMR2), 90–98 (2013).
34. King, N. S. P. *et al.* An 800 MeV proton radiography facility for dynamic experiments. *Nuclear Instruments and Methods in Physics Research A* **424**, 84–91 (1999).
35. Morris, C., Hopson, J. W. & Goldstone, P. Proton radiography. *Los Alamos Science* **30**, 32–45 (2006).
36. Morris, C. L. *et al.* Charged particle radiography. *Reports on Progress in Physics* **76**(046301), 1–26 (2013).
37. Rigg, P. A. *et al.* Proton radiography and accurate density measurements: a window into shock wave processes. *Physical Review B* **77**(220101R), 1–4 (2008).
38. Mottershead, C. T. & Zumbro, J. D. Magnetic optics for proton radiography. in *Proceedings of the 1997 Particle Accelerator Conference,* eds. Comyn, M., Craddock, M. K., Reiser, M. & Thomson Vancouver, J. B. C. Canada, May 12–16, vol. **2**, 1397–1399 (1998).
39. Merrill, F. E. *et al.* Magnifying lens for 800 MeV proton radiography. *Review of Scientific Instruments* **82**(103709), 1–6 (2011).
40. Ansara, I. *et al.* (1994), *CALPHAD: Comput. Coupling Phase Diagrams Thermochem. Al-In Phase Diagram, ASM Alloy Phase Diagrams Center,* eds. Villars, P., Okamoto, H. & Cenzual, K. ASM International, Materials Park, OH. Retrieved December 21, 2012, from http://www1.asminternational.org/AsmEnterprise/APD.
41. Kaban, I., Curiotto, S., Chatain, D. & Hoyer, W. Surfaces, interfaces and phase transitions in Al-In monotectic alloys. *Acta Materialia* **58**, 3406–3414 (2010).
42. Morris, C. L. *et al.* Qualitative comparison of bremsstrahlung x-rays and 800 MeV protons for tomography of urania fuel pellets. *Review of Scientific Instruments* **84**(023902), 1–7 (2013).
43. *Materials Genome Initiative for Global Competitiveness,* Executive Office of the President of the United States, National Science and Technology Council, 2011. Retrieved May 20, 2013, from http://www.whitehouse.gov/sites/default/files/microsites/ostp/materials_genome_initiative-final.pdf.
44. *From Quanta to the Continuum: Opportunities for Mesoscale Science* A Report for the Basic Energy Sciences Advisory Committee Mesoscale Science Subcommittee, U.S. Department of Energy, 2012. Retrieved May 20, 2013, from http://science.energy.gov/~/media/bes/pdf/reports/files/OFMS_rpt.pdf.
45. Crabtree, G. W. & Sarrao, J. L. Opportunities for mesoscale science. *MRS Bulletin* **37**, 1079–1088 (2012).
46. Mottershead, T. *et al.* Design and operation of a proton microscope for radiography at 800 MeV. in *Proceedings of the 2003 Particle Accelerator Conference,* ed. Chew, J., Lucas, P. & Webber, S. Portland, OR, USA, May 12–16, vol. **1**, 702–704 (2003).
47. Valdiviez, R. *et al.* The mechanical design of a proton microscope for radiography at 800 MeV. in *Proceedings of the 2003 Particle Accelerator Conference,* ed. Chew, J., Lucas, P. & Webber, S. Portland, OR, May 12–16, vol. **3**, 1664–1666 (2003).

Acknowledgments

We thank the proton radiography team (LANL) for providing support during these experiments and T.V. Beard, R.W. Hudson, B.S. Folks, D.A. Aragon, T. Wheeler, P.K. Kennedy, and M.P. Maez for providing machining support (LANL). We also thank D.A. Korzekwa, D.L. Hammon, R.R. Trujillo, S.W. Quintana, R.L. Edwards, D.F. Knowlton, A.M. Kelly, J.J. Hill, F. O'Neill, and M.G. Emigh for helping to prepare for the proton radiography experiments and appreciate the helpful advice we received from J.C. Foley, R.M. Aikin and P.S. Dunn (LANL). We gratefully acknowledge the support of the U.S. Department of Energy (DOE) through the LANL/LDRD Program for this work. A.C., S.I., P.G. and M.B. gratefully acknowledge support from A.C.'s Early Career award from the U.S. DOE, Office of Basic Energy Sciences, Division of Materials Sciences and Engineering. Use of the Advanced Photon Source, an Office of Science User Facility operated for the U.S. DOE Office of Science by Argonne National Laboratory, was supported by the U.S. DOE under Contract No. DE-AC02-06CH11357; x-ray data were collected at the Sector 32-ID-C beamline.

Author contributions

A.C., J.C., C.M., F.M., B.H., F.M., T.O., M.B. and T.T. performed the proton radiography experiments. A.C., J.C., T.T., B.P., W.-K.L., K.F. and A.D. performed the synchrotron x-ray radiography experiments. A.C., J.C., T.O., M.B. and T.T. designed and prepared hardware for these experiments. J.C., T.O., M.B., T.T., A.C. and K.C. prepared metallic alloy samples. S.I., J.M., R.F. and T.O. performed microscopy. A.C., S.I., P.G., J.C., K.C., R.F., D.T., J.S. and D.T. contributed to the study design and concepts presented here. A.C., S.I. and P.G. wrote the paper and incorporated comments and contributions from all of the authors.

Additional information

Supplementary information accompanies this paper at http://www.nature.com/scientificreports

Competing financial interests: The authors declare no competing financial interests.

How to cite this article: Clarke, A. *et al*. Proton Radiography Peers into Metal Solidification. *Sci. Rep.* **3**, 2020; DOI:10.1038/srep02020 (2013).